

2D Hopping at Full Frustration: A Numerical Study

Yusuf A. Kinkhabwala, Viktor A. Sverdlov, and Konstantin K. Likharev
*Department of Physics and Astronomy,
Stony Brook University, Stony Brook, NY 11794-3800*

Alexander N. Korotkov
*Department of Electrical Engineering,
University of California - Riverside, Riverside, CA 92521*

(Dated: February 7, 2020)

We have carried out extensive Monte Carlo simulations of 2D hopping (with negligible Coulomb interaction) in a system with a completely random distribution of localized sites in both space and energy, within a broad range of the applied electric field E and temperature T , both within and beyond the variable-range-hopping region. The calculated properties include dc current, statistics of localized site occupation and hop lengths, and current fluctuation spectrum. Within the calculation accuracy, the model does not exhibit $1/f$ noise, so that the low-frequency noise at low temperatures may be characterized by the Fano factor F . For sufficiently large samples, F scales with conductor length L as $(L_c/L)^\alpha$, where $\alpha = 0.76 \pm 0.08$. The electric field dependence of parameter L_c (interpreted as the average percolation cluster length) is compatible with the law $L_c \propto E^{-0.911}$ following from percolation theory arguments at relatively low E , but flattens and approaches the average hop length in very high fields.

PACS numbers: 72.20.Ee, 72.20.Ht, 73.50.Td

I. INTRODUCTION

Theory of hopping transport in disordered conductors,^{1,2,3} without account of electron-electron interaction, is considered a well established (if not completed) field, the recent research being focused mostly on Coulomb effects. Two factors, however, have motivated us to have a new look at this subject:

1. The literature is surprisingly scarce of quantitative data on major characteristics of hopping, especially in the high-electric-field region ($eEr_{rms} \gtrsim k_B T$) where dc conductivity becomes a substantial function of E . To the best of our knowledge, the exact location of the crossover to field-independent conductivity (at finite temperature) has never been established. This is not very surprising because virtually the only theoretical technique available for hopping characterization in the high-field region is Monte Carlo modelling, which requires high-performance computing. For example, the work reported below took about a million processor-hours on modern supercomputers. Such computing resources have become available for the academic solid state physics community only recently.

2. Relatively recently it was recognized that shot noise⁴ is a very important characteristic of electron transport. In particular, the suppression of current fluctuation density $S_I(\omega)$ at low frequencies, relative to its Schottky formula value $2e \langle I \rangle$, is a necessary condition for the so-called sub-electron (quasi-continuous) charge transfer.⁵ Preliminary calculations of shot noise at 1D⁶ and 2D⁷ hopping have shown that such suppression may, indeed, take place. However, the calculations of this effect for

the most important 2D case have been limited to just one particular value of electric field at zero temperature.⁷ It was important to examine whether the law governing this suppression is really as general as it seemed. Such examination, carried out in this work, has become possible only after the development of a new, advanced method of spectral density calculation - see Appendix A.

II. MODEL

We have studied 2D rectangular ($L \times W$) samples with “open” boundary conditions on the interface with well-conducting electrodes⁷ - see inset in Fig. 1. In the present study, we have concentrated on broad samples with width $W \gg L_c$, where L_c is the effective percolation cluster size (see below). The conductor is assumed to be “fully frustrated”: the localized sites are randomly distributed over the sample area, and their energies ϵ_j are randomly distributed over a sufficiently broad energy band, so that the 2D density of states ν is constant at all energies relevant for conduction. Electrons can hop from any site j to any other site k with the rate

$$\gamma_{jk} = \Gamma_{jk} \exp\left(-\frac{r_{jk}}{a}\right). \quad (1)$$

Such exponential dependence on the hop length has been assumed in virtually all theoretical studies of hopping.⁸ However, in contrast to most other authors, we take Eq. (1) literally even at small distances $r_{jk} \sim a$;

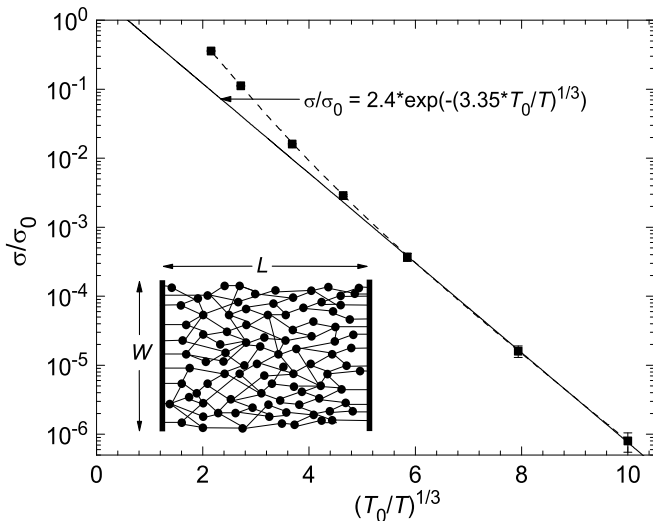


FIG. 1: Linear conductivity σ as a function of temperature T . Points show the results of averaging over 80 samples varying in size ($L \times W$) from $20 \times 10a^2$ to $160 \times 100a^2$, biased by a low electric field $E \ll E_T$. Points are Monte Carlo results. The dashed line is just a guide for the eye, while the straight line corresponds to the best fit of the data by Eq. (6). Constants T_0 and σ_0 are defined by Eqs. (4) and Eq. (5), respectively. The inset shows the system under analysis (schematically).

this is important only at very high fields and/or temperatures where the average value of r_{jk} becomes comparable to a . Of course our quantitative results for this region are only true for specific confining potentials providing an exponential wave function decay.

Another distinction from some other works in this field is that we assume that the hopping rate amplitude Γ_{jk} depends continuously on the localized site energy difference $\epsilon_{jk} \equiv \epsilon_j - \epsilon_k + e\mathbf{E}r_{jk}$:

$$\hbar\Gamma_{jk}(\epsilon_{jk}) = g \frac{\epsilon_{jk}}{1 - \exp\left(-\frac{\epsilon_{jk}}{k_B T}\right)}. \quad (2)$$

This model coincides, for low phonon energies ϵ_{jk} , with that described by Eqs. (4.2.17)-(4.2.19) of Ref. 2, and of course satisfies the Gibbs detailed balance requirement $\Gamma_{jk} = \Gamma_{kj} \exp(\epsilon_{jk}/k_B T)$. It is also close, but in our view, more natural than the ‘‘Metropolis’’ dependence with a cusp at $\epsilon_{jk} = 0$.

The interaction of hopping electrons is assumed negligible, with the exception of the implicit Pauli-principle interaction, i.e. no hopping to already occupied sites.

Scales of all variables within our model are natural combinations of the constants a and ν (plus temperature T , applied electric field E , and fundamental constants). In particular, there are three possible energy scales: $k_B T$, eEa , and $(\nu a^2)^{-1}$. This means that there are two characteristic values of electric field:

$$E_T \equiv \frac{k_B T}{ea}; E_0 \equiv \frac{1}{e\nu a^3}. \quad (3)$$

We will be mostly interested in the case of low temperatures, $T < T_0$, where

$$T_0 \equiv \frac{1}{k_B \nu a^2} \quad (4)$$

is the field-independent scale of temperature, so that $E_T < E_0$.

Note that the only role of the dimensionless parameter g introduced by Eq. (2) is to participate in the scale of hopping conductivity

$$\sigma_0 \equiv g \frac{e^2}{\hbar}. \quad (5)$$

In order to keep coherent quantum effects leading to weak localization and metal-to-insulator transition negligibly small, and hence the formulated hopping model possible, g should be much less than unity.

The dynamic Monte Carlo calculations were carried out using the algorithm suggested by Bakhvalov et al.,⁹ which has become the de facto standard for single-electron tunnelling simulations.¹⁰ All calculated variables were averaged over the sample, and in most cases, over several (many) samples with independent random distributions of localized sites in space and energy, but with the same dimensionless parameters L/a , W/a , T/T_0 , and E/E_0 . For the purposes of this work, the noise, i.e. current spectral density, calculation technique has been modified (see Appendix A).

III. DC CURRENT AND HOPPING STATISTICS

In order to understand the relation between our model and the prior results in this field, we have started from the calculation of dc current $\langle I \rangle$ as a function of T and E . If the electric field is small, $E \ll E_T$, then the current is proportional to E , and the transport is completely characterized by the linear conductivity $\sigma \equiv \langle I \rangle / WE$. Fig. 1 shows the calculated conductivity as a function of temperature T ; in the whole region $T \ll T_0$ this dependence follows the 2D Mott law^{1,2,3}

$$\sigma = A_T \sigma_0 \exp\left[-\left(B_T \frac{T_0}{T}\right)^{1/3}\right], \quad (6)$$

within the accuracy of our numerical experiments. For the constants participating in this expression, fitting gives the following values

$$A_T = 2.4 \pm 0.1; B_T = 3.35 \pm 0.12. \quad (7)$$

This result for B_T should be compared with the following values reported in the literature: ~ 2.2 ,¹¹ 3.45 ,² and 3.25 .¹² The differences are possibly due to that of the slightly different models for the function $\Gamma_{jk}(\epsilon_{jk})$ (see Sec. II above).

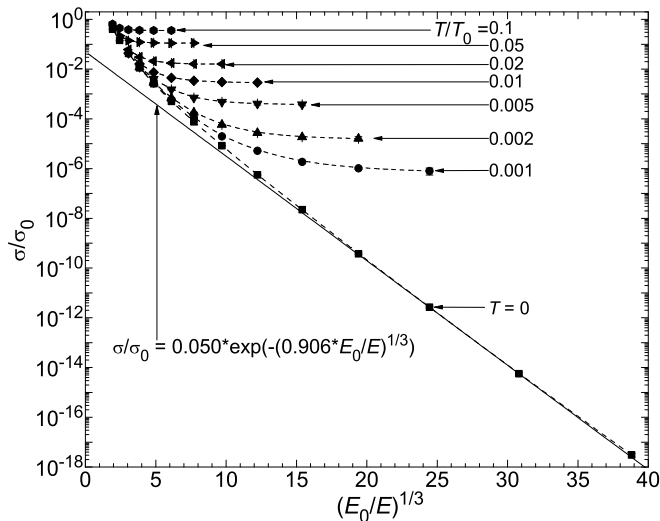


FIG. 2: Nonlinear conductivity $\sigma \equiv \langle I \rangle / WE$ as a function of electric field E for several values of temperature T . Each point represents data averaged over 80 samples of the same size (ranging from $20 \times 14a^2$ to $1000 \times 700a^2$, depending on T and E). Points are Monte Carlo results. Dashed lines are only guides for the eye, while the straight line shows Eq. (8) with the best-fit values of A_E and B_E .

At higher electric fields ($E \gtrsim E_T$), dc current starts to grow faster than the Ohm law, so that if we still keep the above definition of conductivity σ , it starts to grow with E (Fig. 2). At $T \rightarrow 0$, the results are well described by the “high-field” equation¹⁵

$$\sigma = A_E \sigma_0 \exp \left[- \left(B_E \frac{E_0}{E} \right)^{1/3} \right], \quad (8)$$

with

$$A_E = 0.050 \pm 0.005; B_E = 0.906 \pm 0.015. \quad (9)$$

These values present an improvement on Ref. 7 where $A_E = 1.1$ and $B_E = 1.27$ had been determined from a narrower range of electric fields.

Finally, Fig. 2 shows that when the electric field becomes comparable with the value E_0 defined by the second of Eqs. (3), dc current and hence, conductivity start to grow even faster than given by Eq. (8).

In order to understand the physics of hopping in these three field regions better, it is very useful to have a look at the statistics of localized site occupation and hopping length. We have found that for all studied values of E and T , the probability of site occupation closely follows the Fermi distribution with the local Fermi level

$$\mu(\mathbf{r}) = \mu_L - e\mathbf{E}\mathbf{r} \quad (10)$$

(where μ_L is the Fermi level of the source electrode) and some effective temperature T_{ef} . Points in Fig. 3 show T_{ef} as a function of electric field E for several values of physical temperature T . Dashed lines show the result of the

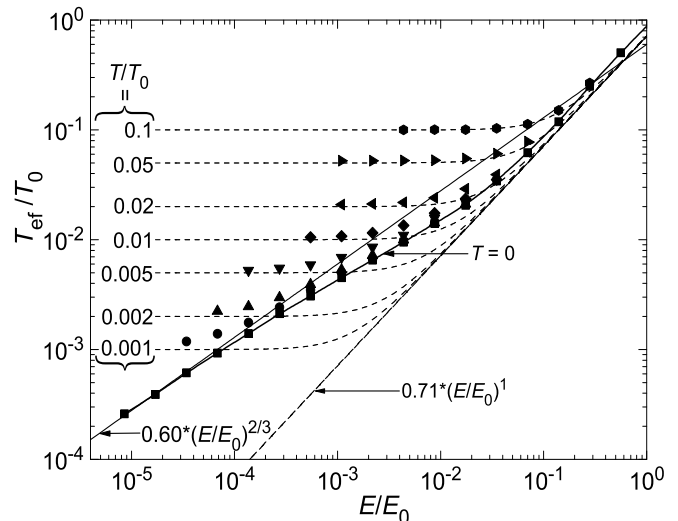


FIG. 3: The effective temperature T_{ef} of current carriers as a function of electric field E for several values of temperature T . Closed points: Monte Carlo (MC) simulation results; dashed lines: master equation (ME) results. The solid curve marked $T = 0$ is only a guide for the eye.

best fitting of the naive single-particle master equation

$$\begin{aligned} \frac{\partial f(\epsilon, t)}{\partial t} = & \int d^2r \int d\epsilon' \exp\left(\frac{-r}{a}\right) \\ & \times \{ -\Gamma(\epsilon - \epsilon' + e\mathbf{E}\mathbf{r}) f(\epsilon) [1 - f(\epsilon')] \\ & + \Gamma(\epsilon' - \epsilon - e\mathbf{E}\mathbf{r}) f(\epsilon') [1 - f(\epsilon)] \} \quad (11) \end{aligned}$$

by a stationary Fermi distribution. Equation (11) would follow from our model if percolation effects were not substantial. At real hopping, we can expect the results following from Eq. (11) to be valid only in certain limits.¹³ For example, in the low field limit, $E \rightarrow 0$, both methods give $T_{ef} = T$. At higher fields the effective temperature grows with the applied field, which “overheats” the electrons. At very high fields ($E/E_0 \gtrsim 0.3$) both methods agree again and give

$$k_B T_{ef} \approx C e E a, \quad C = 0.71 \pm 0.02. \quad (12)$$

(A similar result, but with $C \approx 1.34$, for our definition of a , was obtained by Marianer and Shklovskii¹⁴ for a rather different model with an exponential energy dependence of the density of states ν .) However, at the intermediate fields $E_T \ll E \ll E_0$ (this regime is frequently called the “high-field variable-range-hopping”), the master equation still gives the same result (12) and hence fails to appreciate that in fact T_{ef} is proportional to $E^{2/3}$. In order to explain this result, let us discuss the statistics of hop lengths (Figs. 4 and 5).

The two- and one-dimensional histograms in Fig. 4 show the probability density P of a hop between two sites separated by the vector $\Delta\mathbf{r}$, and also the density P_d weighed by the factor $|N_{jk} - N_{kj}|$, where each N is the

total number of hops (during a certain time interval) in the indicated direction. The latter weighing emphasizes the site pairs (j, k) contributing substantially to the net hopping transport, in comparison with “blinking” site pairs, which exchange an electron many times before allowing it to advance along the field. It is clear that at relatively high temperatures or low fields ($E \ll E_T$) the non-weighted distribution should be symmetric (Fig. 4a). Fig. 4d shows that in this case the one-dimensional probability density is well approximated by the Rayleigh distribution, $P(r) \propto r \exp(-r/a)$. However, the weighed hop distribution is strongly asymmetric even in the limit $E \rightarrow 0$ (Fig. 4b). This asymmetry is even more evident at low temperatures or high fields ($E \gg E_T$); in this case the distribution has a sharp boundary (Fig. 4c). Fig. 4d shows those cases where the 1D histograms deviate substantially from the distribution predicted by the master equation (see Eq. (19)).

Figure 5 shows the r.m.s. non-weighted (r_{rms}) and direction-weighted (r_{rmds}) hop lengths, defined, respectively, as

$$r_{rms} \equiv \frac{\sum_{j,k} (r_{jk}^2 N_{jk} + r_{kj}^2 N_{kj})}{\sum_{j,k} (N_{jk} + N_{kj})} \quad (13)$$

and

$$r_{rmds} \equiv \frac{\sum_{j,k} |r_{jk}^2 N_{jk} - r_{kj}^2 N_{kj}|}{\sum_{j,k} |N_{jk} - N_{kj}|} \quad (14)$$

(that are of course just the averages of the histograms shown in Fig. 4), as functions of applied electric field for several values of temperature. At $T \rightarrow 0$, hopping is strictly one-directional (i.e., if $N_{jk} \neq 0$, then $N_{kj} = 0$), so that r_{rms} and r_{rmds} should be equal. In fact, simulation shows that in this limit both lengths coincide, at lower fields following the scaling¹⁵

$$r_{rms} = r_{rmds} = Da \left(\frac{E_0}{E} \right)^{1/3}, \quad E_T \ll E \ll E_0, \quad (15)$$

with $D = 0.72 \pm 0.01$. (We are not aware of any prior results with which this value could be compared.)

This scaling of r in the variable-range-hopping region is essentially the reason for the scaling of T_{ef} mentioned above; in fact, the hopping electron gas “overheating” may be estimated by equating $k_B T_{ef}$ to the energy gain $e\mathbf{E}\mathbf{r}_{rms}$, possibly multiplied by a constant of the order of one. For the effective temperature, this estimate gives

$$k_B T_{ef} = const \times e\mathbf{E}\mathbf{r}_{rms} = GeaE_0^{1/3} E^{2/3} = G \frac{(E/E_0)^{2/3}}{va^2}, \quad (16)$$

in accordance with the result shown in Fig. 3. For constant G our Monte Carlo simulations give the value 0.60 ± 0.02 ; we are not aware of any previous results this number could be compared with.

At higher fields ($E \gtrsim 0.1E_0$) the hop lengths start to decrease slower, approaching a few localization lengths a (Fig. 5a). In this (“ultra-high-field”) region, the energy range $\sim eEa$ for tunnelling at distances of a few a is so high that there are always some accessible empty sites within this range, so that long hops, so dominant at variable range hopping, do not contribute much into conduction.

At finite temperatures, the most curious result is a non-monotonic dependence of the r.m.s. hopping length on the applied field - see Fig. 5a. At $E \rightarrow 0$, r_{rms} has to be field-independent, and there is no scale for it besides a . (As evident as it may seem, this fact is sometimes missed in popular descriptions of hopping.) In order to make a crude estimate of r_{rms} in this limit, one can use the master equation Eq. (11). In this approach, at thermal equilibrium (i.e. at Γ independent of r), the hop length probability density $P(r)$ can be found as

$$P(r) = 2\pi r \int d\epsilon \int d\epsilon' \exp\left(\frac{-r}{a}\right) \times \{ \Gamma(\epsilon - \epsilon') f(\epsilon) [1 - f(\epsilon')] + \Gamma(\epsilon' - \epsilon) f(\epsilon') [1 - f(\epsilon)] \} \propto r \exp\left(\frac{-r}{a}\right), \quad (17)$$

in a good agreement with the results shown in Fig. 4d for this case. From Eq. (17), we get

$$r_{rms} \equiv \langle r^2 \rangle^{1/2} = \left[\frac{\int P(r) r^2 dr}{\int P(r) dr} \right]^{1/2} = \sqrt{6}a \approx 2.45a, \quad (18)$$

in a good agreement with numerical data shown in Fig. 5.

A similar calculation for r_{rmds} may be obtained by expanding the tunnelling rate $\Gamma(\epsilon - \epsilon' + e\mathbf{E}\mathbf{r})$ in small electric field as $\Gamma(\epsilon - \epsilon') + e\mathbf{E}\mathbf{r}\Gamma'(\epsilon - \epsilon')$. The result is

$$P_d(r) = eEr^2 \int d\phi |\cos\phi| \int d\epsilon \int d\epsilon' \exp\left(\frac{-r}{a}\right) \times \{ \Gamma'(\epsilon' - \epsilon) f(\epsilon') [1 - f(\epsilon)] + \Gamma'(\epsilon - \epsilon') f(\epsilon) [1 - f(\epsilon')] \},$$

$$P_d(r) \propto r^2 \exp\left(\frac{-r}{a}\right),$$

$$r_{rmds} \equiv \left[\frac{\int P_d(r) r^2 dr}{\int P_d(r) dr} \right]^{1/2} = \sqrt{12}a \approx 3.46a. \quad (19)$$

The Monte Carlo data (Fig. 5), however, differ from this result, showing that at $E \rightarrow 0$, r_{rmds} obeys the Mott law^{1,2,3}

$$r_{rmds} = Ha \left(\frac{T_0}{T} \right)^{1/3} + Ia, \quad T \ll T_0, \quad (20)$$

with the best-fit values $H = 0.52 \pm 0.05$ and $I = 2.0 \pm 0.1$.¹⁶ In contrast, the function $r_{rms}(T)$ is rather far from Eq. (20), because the Mott law refers to long

hops responsible for transport (with the average approximately corresponding to r_{rms}), while r_{rms} reflects the statistics of all hops.

To summarize, our results for average conductivity and hop statistics confirm that our model gives a reasonable description of the well-known picture of hopping, including the usual variable range hopping at low fields ($E \ll E_T$) and “high-field variable range hopping” at $E_T \ll E \ll E_0$. Moreover, the model also describes the “ultra-high field” region ($E \sim E_0$) where the variable range hopping picture is no longer valid, since from most localized sites an electron can hop, with comparable probability, to several close sites. In the last region, there is no single percolation cluster isolated in the sample; rather, electrons follow a large number of interwoven trajectories.

IV. SHOT NOISE

The achieved understanding of hopping (within our model) has helped us to interpret the results of current noise simulation. This simulation was limited to the case of low temperatures, $E_T \ll E$. (In the opposite limit, noise is described by the fluctuation-dissipation theorem, its low-frequency intensity can be found from $\sigma(T)$ and does not require a special calculation.)

The largest practical problem with the noise evaluation is that the calculation of spectral density $S_I(\omega)$ of current fluctuations with acceptable accuracy typically requires much larger statistical ensemble of random samples than that of the average current. This is why, even with an advanced algorithm for spectral density calculation (see Appendix A), noise calculation has required very substantial supercomputer resources.

Figure 6 shows a typical dependence of the current noise spectral density S_I on the observation frequency ω . One can see a smooth crossover from high-frequency to low-frequency noise, that is typical for systems with single-electron tunnelling - see, e.g., Refs.(6,7,17,18,19). At even lower frequencies, a crossover to $1/f$ noise might be expected, because the discussion of this effect in some earlier publications^{20,21} was apparently independent of the Coulomb interaction between hopping electrons. However, within the accuracy of our simulations, we could not find any $1/f$ -type noise for any parameters we have explored.

Since the low-frequency spectral density is flat, it may be characterized by the Fano factor

$$F \equiv \frac{S_I(0)}{2e\langle I \rangle}, \quad (21)$$

which is the commonly accepted characterization of shot noise.⁴ Figure 7 shows the average Fano factor as a function of L for several values of the applied electric field. This figure shows that the results may be reasonably well fit with a universal dependence on L/L_c , that

approaches⁷

$$\langle F \rangle = \left(\frac{L_c}{L} \right)^\alpha, \quad L \gg L_c. \quad (22)$$

Here α is a numerical exponent; in the current study we could establish that

$$\alpha = 0.76 \pm 0.08. \quad (23)$$

This is compatible with our previous results⁷ $\alpha = 0.85 \pm 0.07$ (for the same model as now, for one particular value of E) and $\alpha = 0.85 \pm 0.02$ (for nearest neighbor hopping on uniform slanted lattices).

Figure 8 shows the fitting parameter L_c (as well as the average hop length along the electric field, x_{rms}) as a function of electric field E . In the variable range hopping region, it may be fitted with the following law,

$$L_c = Ja \left(\frac{E_0}{E} \right)^\mu, \quad J = 0.04 \pm 0.01, \mu = 0.98 \pm 0.08. \quad (24)$$

This law may be interpreted in the following way. The parameter L_c is essentially the average percolation cluster length.⁷ The theory of directed percolation^{22,23,24} gives the following scaling:

$$L_c \propto \langle x \rangle \left(\frac{x_c}{|\langle x \rangle - x_c|} \right)^{\nu_{\parallel}}. \quad (25)$$

Here $\langle x \rangle$ is the r.m.s. hop length along the field direction, x_c is its critical value, and the critical index ν_{\parallel} should be close to 1.73.²⁴ Due to the exponential nature of the hopping, $|\langle x \rangle - x_c| \sim a$, while $\langle x \rangle$ should follow field scaling similar to that given by Eq. (15). (Square points in Fig. 8 show that this is true for our simulation results as well.) Thus for sufficiently large $\langle x \rangle$ we arrive at Eq. (24) with $\mu = \frac{1}{3}(1 + \nu_{\parallel}) \approx 0.911$. This value is compatible with our numerical result, thus confirming the interpretation of L_c as the average percolation cluster length.

Note that in the variable range hopping regime L_c has a different field dependence, and is much larger than the average hop length. However, as the applied electric field approaches E_0 , both lengths become comparable with each other and with the localization radius a .

V. DISCUSSION

Our simulations of shot noise at 2D hopping have confirmed our earlier hypothesis⁷ that in the absence of substantial Coulomb interaction, in sufficiently large samples ($L, W \gg L_c$) the Fano factor F scales approximately proportionally to $1/L$ - see Eq. (22). Other confirmations of this hypothesis have come from recent experiments with lateral transport in SiGe quantum wells²⁵ and GaAs MESFET channels.²⁶ Unfortunately, these experiments are not precise enough to distinguish the small difference between the exponent α in Eq. (22) from unity.

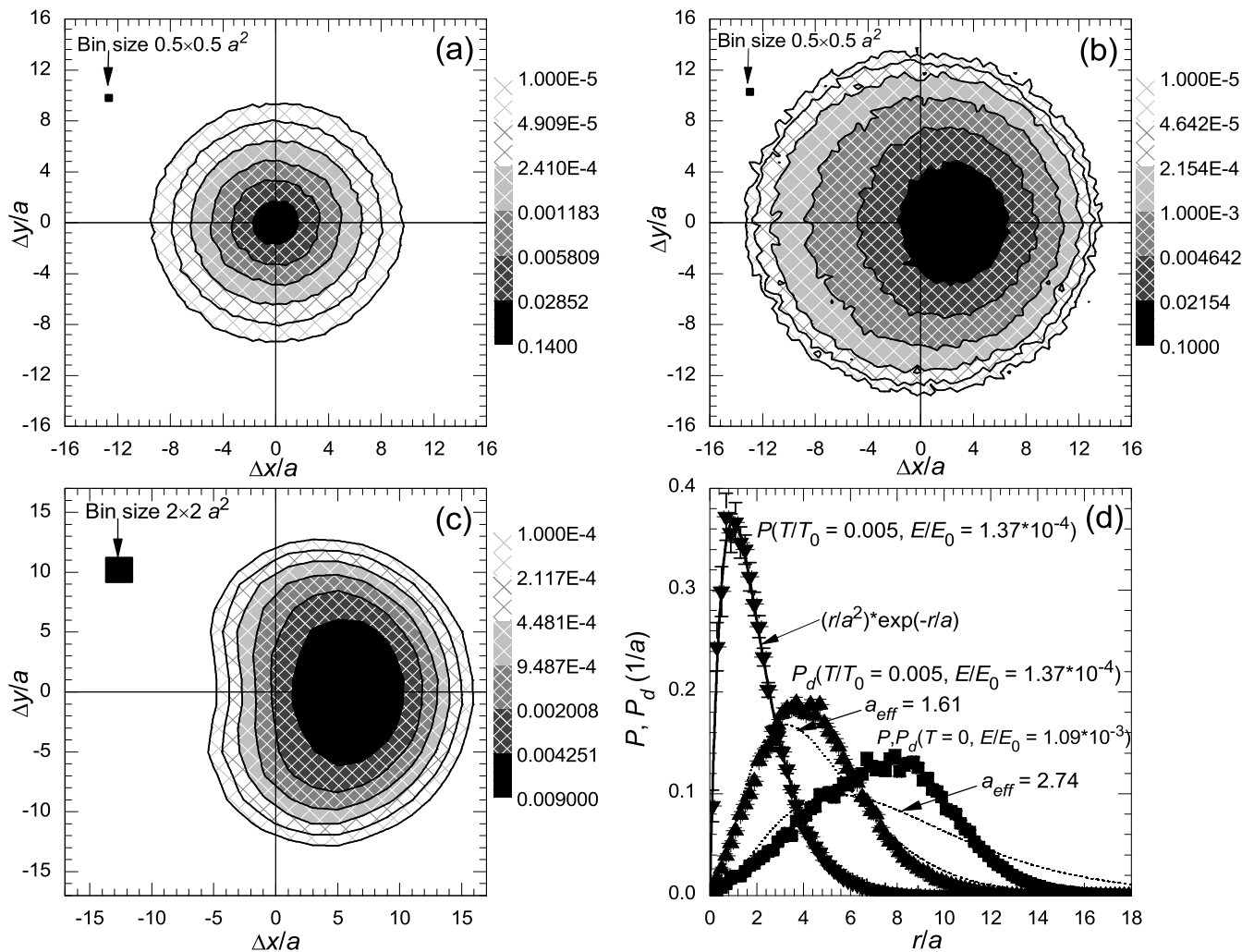


FIG. 4: (a)-(c) Two-dimensional and (d) one-dimensional histograms of hop lengths for two typical cases: (a) and (b): $T/T_0 = 5 \times 10^{-3}$, $E/E_0 = 1.37 \times 10^{-4}$ ($E \ll E_T$) and (c): $T = 0$, $E/E_0 = 1.09 \times 10^{-3}$ ($E_T \ll E$). The vertical (shade-coded) scale in panels (a) and (c) is proportional to the probability P of hops with given $\Delta \mathbf{r} = (\Delta x, \Delta y)$, while that in panel (b), to the probability P_d weighed by factor $|N_{jk} - N_{kj}|$ - see the text. (Since at $T = 0$ there are no backward hops, for the case shown in panel (c), P and P_d coincide.) Panel (d) shows P and P_d , averaged over all angles of vector $\Delta \mathbf{r}$, for both the high-field and low-field case. Dashed lines show the distribution (19) given by master equation, for best-fit values of a_{eff} .

The hypothesis that α is in fact equal to 1 for sufficiently long samples seems appealing, because it would mean the simple addition of mutually-independent noise voltages generated by sample sections connected in series. On the contrary, a deviation of α from unity would mean that dynamic correlations of electron motion in percolation clusters persist even at $L \gg L_c$. We can present, as an example, at least one exactly solvable model (the “asymmetric single exclusion process”, or ASEP²⁷) in which the dynamic correlations may change α from 1 to 0.5. (It is instructive to notice that in the ASEP model the dynamic correlations do not affect average transport characteristics, and may be ignored, in particular, in calculations of dc current.) One more remark we can offer is that the value of α following from our calculations (0.76)

does not violate any scaling laws. On the other hand, at this stage we cannot exclude the possibility that α will tend closer to one (say, logarithmically) in extremely long samples.

From the point of view of possible applications in single-electron devices,²⁸ the fact that F may be suppressed to values much less than unity, may seem encouraging, since it enables the use of circuit components with quasi-continuous charge transport for the compensation of random background charge in single-electron islands. However, in order to achieve the really quasi-continuous transfer (say, $F \lesssim 0.1$), the sample length L has to be an order of magnitude longer than the percolation cluster length scale L_c . On the other hand, L_c itself, especially in the most interesting case of low applied field, is much

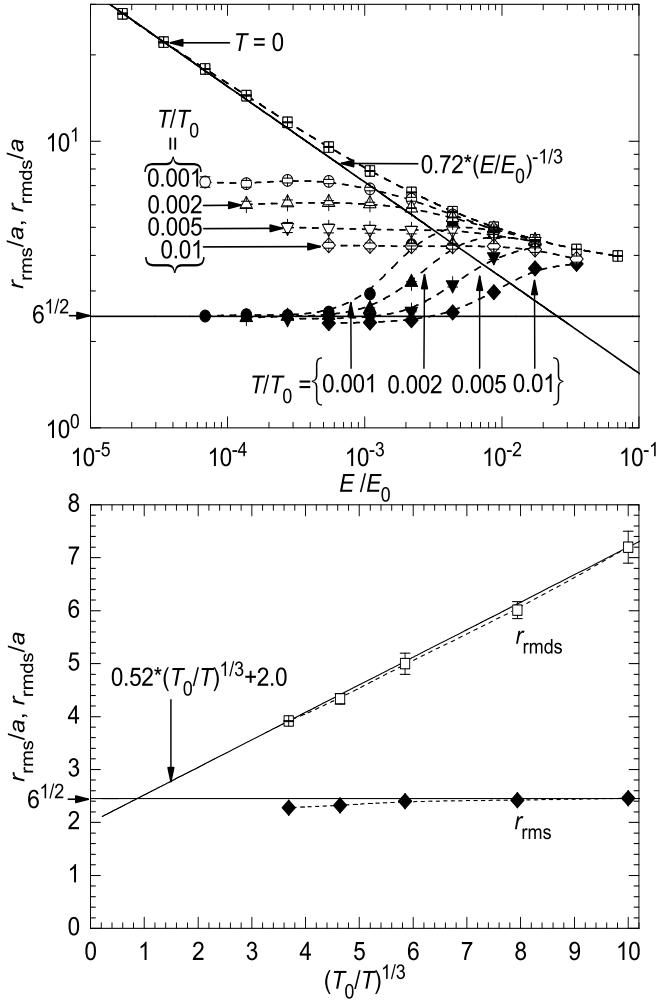


FIG. 5: R.m.s. hop length r_{rms} (solid points) and the weighed average length r_{rms} (open points) as functions of (a) applied electric field E for several temperatures T , and (b) of temperature at $E \rightarrow 0$. Tilted straight lines in panels (a) and (b) show the best fits by Eqs. (15) and (20), respectively, while the horizontal thin lines show the values following from the master equation. Curves are only guides for the eye.

longer than the localization length a (Fig. 8), which is of the order of 1 nm in most prospective materials. Hence, it may be hard to implement sub-electron transport in components substantially smaller than 100 nm. This size is probably too large for future room-temperature single-electron circuits,²⁸ because of large stray capacitance that effectively adds up to the capacitance of the island to be serviced.

Acknowledgments

Fruitful discussions with B. Shklovskii and D. Tsankov are gratefully acknowledged. The work was supported in part by the Engineering Physics Program of the Office of Basic Energy Sciences at the U.S. Department

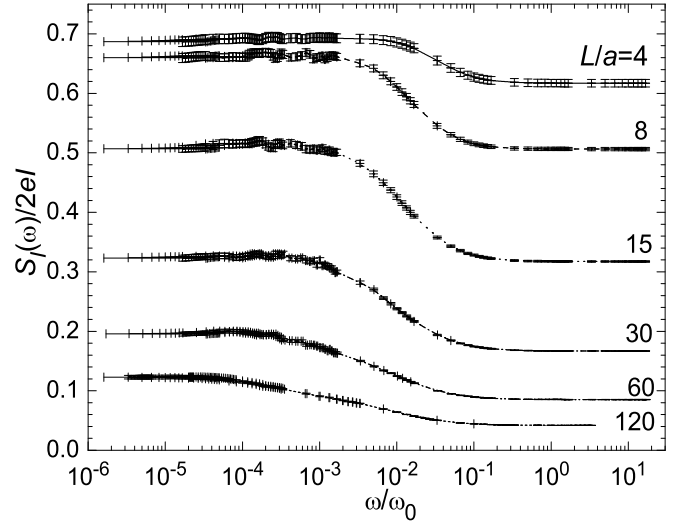


FIG. 6: Spectral density S_I of current fluctuations as a function of observation frequency ω , measured in units of $\omega_0 = (I/e)/(W/a)$, for several values of sample length L . Parameters: $E/E_0 = 8.75 \times 10^{-3}$, $W/a = 60$, $T = 0$. Lines are only guides for the eye.

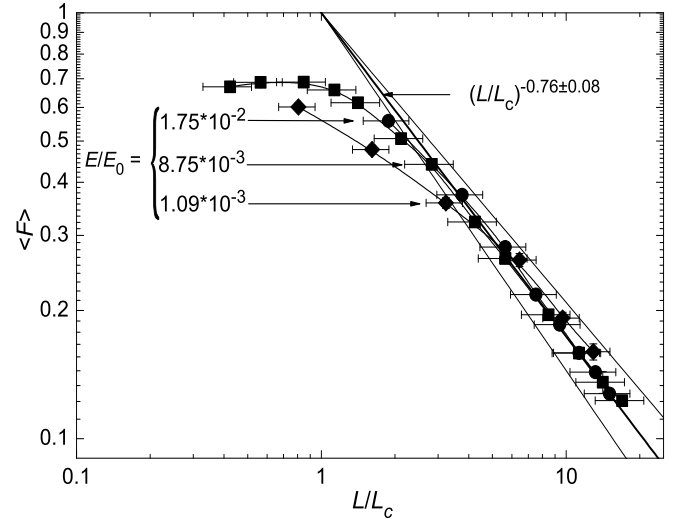


FIG. 7: Average Fano factor $\langle F \rangle$ as a function of sample length L normalized on the average cluster size L_c (see Fig. 8 below), for several values of applied field. $T = 0$, $W \gg L_c$.

of Energy. We also acknowledge the use of the following supercomputer resources: SBU's cluster *Njal* (purchase and installation funded by U.S. DoD's DURINT program), Oak Ridge National Laboratory's IBM SP computer *Eagle* (funded by the Department of Energy's Office of Science and Energy Efficiency program), and also IBM SP system *Tempest* at Maui High Performance Computing Center and IBM SP system *Habu* at NAVO Shared Resource Center (computer time granted by DOD's High Performance Computing Modernization

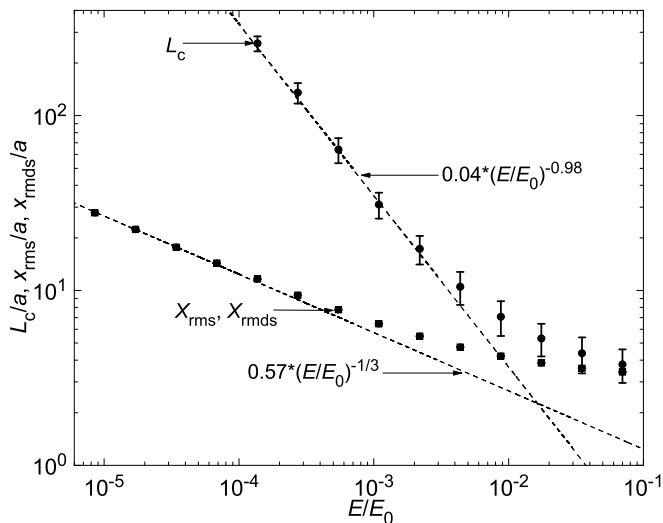


FIG. 8: The value of L_c giving the best fitting of shot noise results by Eq. (22) as a function of applied electric field (solid circles). solid squares show the simple and direction-weighted average hop length along the applied field direction, defined similarly to Eqs. (13) and (14).

Program).

APPENDIX A: ALGORITHM FOR CURRENT SPECTRAL DENSITY CALCULATION

In this Appendix we describe the numerical algorithm used for the Monte Carlo calculation of the spectral density $S_I(\omega)$ of the hopping current $I(t)$. (This algorithm has been also used, without explanation, in our earlier papers^{6,7,29}). Besides calculation of noise in hopping, the method is applicable to the spectral density of tunneling current in multi-junction single-electron devices³⁰ because of the problem similarity.

The first spectral calculations of the electron transport in single-electron devices using Monte Carlo technique have been performed in Refs.^{9,17}; in these papers the spectral density has been calculated as a Fourier transform of the correlation function. However, this method is rather slow in the case when the current $I(t)$ is a sequence of δ -functions, corresponding to tunneling events:

$$I(t) = \sum_n q_n \delta(t - t_n), \quad (\text{A1})$$

where t_n is a (random) time of the n -th tunneling event and q_n is the corresponding charge transfer. (The sequence $\{q_n\}$ is also random and reflects the path in the space of charge configurations.)

A significantly faster “standard” algorithm¹⁹ (embedded, for example, into the simulation package MOSES³¹) is based on the definition of the spectral density $S_I(\omega)$ of the current $I(t)$ via the square of the Fourier transform $|I(\omega)|^2$. More specifically, for the rectangular time

window (natural in simulations) there is a relation

$$\begin{aligned} & \frac{2}{T} \left\langle \left| \int_{t_0}^{t_0+T} I(t) \exp(i\omega t) dt \right|^2 \right\rangle \\ &= \int_{-\infty}^{+\infty} S_I(\omega + \Omega) \frac{1 - \cos(\Omega T)}{\pi T \Omega^2} d\Omega \quad (\text{A2}) \end{aligned}$$

(here $\langle \dots \rangle$ denotes ensemble averaging and i in this Appendix is the imaginary unit), whose right hand side tends to $S_I(\omega)$ in the limit $T \rightarrow \infty$. Therefore,

$$\tilde{S}_I(\omega) \equiv \frac{2}{T} \left\langle \left| \sum_n q_n \exp(i\omega t_n) \right|^2 \right\rangle \quad (\text{A3})$$

is a good approximation for the true spectral density $S_I(\omega)$ even for a finite, but large enough time interval T . (Summation in Eq. (A3) is over the tunneling events within the interval $t_0 < t_n < t_0 + T$). In the standard method^{19,31} the ensemble averaging in Eq. (A3) is replaced by averaging over K sequential time segments (each of duration T) of the Monte Carlo realization, so that t_0 becomes jT , where $j = 1, 2, \dots, K$. It is natural to calculate simultaneously the spectral density for a set of frequency points (the set of harmonics of a certain low frequency is most convenient), and it is useful to choose $\omega/2\pi$ equal to integer multiples of T^{-1} to avoid “poisoning” of the right hand side of Eq. (A2) by the δ -function contribution from $S_I(0)$ due to dc current \bar{I} . (Other ways of subtracting the effect of \bar{I} are also possible.)

A major disadvantage of this standard method is that the relative accuracy of the spectral density calculation cannot be better than approximately $K^{-1/2}$, because the right hand side of Eq. (A3) before averaging over K segments has the rms fluctuation comparable to the mean value. It is easy to increase K (without increasing the total simulation time) by decreasing T ; however, besides increasing the smoothing of $S_I(\omega)$ [which is $\Delta\omega \sim T^{-1}$ – see Eq. (A2)], this may lead to incorrect results when T becomes comparable or less than the longest correlation time of the simulated process, and therefore the T -segments are no longer statistically independent. Since the correlation time is not known in advance (it may be estimated as the lowest frequency at which the spectral density levels off), the choice of T is not a trivial task and requires some intuition that complicates the use of the standard method.

Here we describe the advanced algorithm of spectral density calculation which eliminates this problem and also makes calculation significantly faster (for the same accuracy of the result). The method is somewhat similar to the “reduced” method for dc current calculation¹⁹ and basically treats the randomness of tunneling times t_n analytically, while the path in the charge configuration space is still simulated⁹ by the Monte Carlo technique.

Let us consider a T -long realization of the process assuming for simplicity $t_0 = 0$, so that $t_n = \sum_{k=1}^n \tau_k$ where τ_k is the time between the adjacent tunneling events, i.e.

time spent in a particular charge state. In the case when the system parameters (external voltage, etc.) do not change with time, the random time τ_k has the Poisson distribution with the average value $\langle \tau_k \rangle = 1/\Gamma_{k,\Sigma}$, where $\Gamma_{k,\Sigma}$ is the sum of all tunneling rates for the corresponding charge state. The quantity $s \equiv |\sum_n q_n \exp(i\omega t_n)|^2$, which is related to the spectral density via Eq. (A3), may be easily expressed as

$$\begin{aligned} s &= \sum_{n,m} q_n q_m \exp \left[i\omega \left(\sum_{k=1}^n \tau_k - \sum_{k=1}^m \tau_k \right) \right] \\ &= \sum_n q_n^2 + 2 \operatorname{Re} \sum_{n>m} q_n q_m \exp \left[i\omega \sum_{k=m+1}^n \tau_k \right]. \end{aligned} \quad (\text{A4})$$

For the ensemble averaging of s let us first average Eq. (A4) over random τ_k , leaving averaging over paths in charge space for later. Using the mutual independence of τ_k fluctuations, we can average each exponent independently:

$$\langle e^{i\omega \tau_k} \rangle = \int_0^\infty \frac{e^{-\tau/\langle \tau_k \rangle} e^{i\omega \tau} d\tau}{\langle \tau_k \rangle} = \frac{1}{1 - i\omega \langle \tau_k \rangle}, \quad (\text{A5})$$

thus obtaining the expression

$$\langle s \rangle = \sum_n q_n^2 + 2 \operatorname{Re} \left(\sum_{n>m} q_n q_m \prod_{k=m+1}^n \frac{1}{1 - i\omega \langle \tau_k \rangle} \right). \quad (\text{A6})$$

This expression can be calculated iteratively introducing complex variables

$$A_p \equiv \sum_{n=1}^p q_n^2 + 2 \sum_{n>m} q_n q_m \prod_{k=m+1}^n \frac{1}{1 - i\omega \langle \tau_k \rangle}, \quad (\text{A7})$$

$$B_p \equiv \sum_{m=1}^p q_m \prod_{k=m+1}^p \frac{1}{1 - i\omega \langle \tau_k \rangle}, \quad (\text{A8})$$

that satisfy recurrent equations

$$A_{p+1} = A_p + q_{p+1}^2 + 2q_{p+1} B_p \frac{1}{1 - i\omega \langle \tau_{p+1} \rangle}, \quad (\text{A9})$$

$$B_{p+1} = q_{p+1} + B_p \frac{1}{1 - i\omega \langle \tau_{p+1} \rangle}, \quad (\text{A10})$$

with initial condition $A_0 = B_0 = 0$, while $\langle s \rangle = \operatorname{Re} A_p$ at the end of realization.

It is important to notice that $\operatorname{Re} A_p$ accumulates with the length of realization (in contrast to s before averaging, which is a strongly fluctuating variable), so that $(2/\langle t_p \rangle) \operatorname{Re} A_p$ (where $\langle t_p \rangle = \sum_k^p \langle \tau_k \rangle$) tends to some limit at $p \rightarrow \infty$. This is the reason why, in contrast to the standard method, the numerical averaging over many T -segments is not necessary now, and the ensemble averaging of the segments over different realizations can be replaced by the natural ‘‘time’’ averaging over the length of a realization. This eliminates the problem of

choosing T , discussed above, and now T can be treated as a running variable $T_p = \langle t_p \rangle$ during the whole simulation run. Similarly, s can also be treated as a running variable s_p . (Strictly speaking, averaging over τ_k in the segments with a fixed time T and/or a fixed charge path is different; however, the difference vanishes at large T).

Thus, the basic algorithm is the following. The Monte Carlo technique is used to simulate one long realization of the random path in the configuration (charge) space, while the time is treated deterministically as $\sum_k \langle \tau_k \rangle$; the variables A_p and B_p are updated after each tunneling event using Eqs. (A9)–(A10), and the current spectral density $S_I(\omega)$ is calculated as

$$S_I(\omega) \approx \frac{2}{\langle t_p \rangle} \operatorname{Re} A_p. \quad (\text{A11})$$

Even though breaking the simulation into segments is not needed in the new method, the calculation and comparison of partial results for $S_I(\omega)$ on some time segments is useful for run-time estimates of the calculation accuracy.

Actually, this basic algorithm still requires several improvements to become faster than the standard method, especially at low frequencies. First, the accuracy can be significantly improved by explicitly calculating the spectral density for the function $I(t) - \bar{I}$ instead of $I(t)$. (The average current \bar{I} can be calculated as $\sum_k q_k / \sum_k \langle \tau_k \rangle$, which is the same as in the reduced method^{19,31}.) For this purpose the definition of quantity s_p should be modified to $s_p = |[\sum_n^p q_n \exp(i\omega t_n)] - \bar{I} [\exp(i\omega t_p) - 1] / i\omega|^2 = |\sum_n^p \exp(i\omega t_n) [q_n - \bar{I}(1 - \exp(-i\omega \tau_n)) / i\omega]|^2$. From this point, the derivations are similar to those discussed above, though are now significantly lengthier. The final result is that the only change in the algorithm is a different set of recurrent equations replacing Eqs. (A9)–(A10):

$$\begin{aligned} A_{p+1} &= A_p + q_{p+1}^2 - 2\bar{I} \langle \tau_{p+1} \rangle \frac{q_{p+1} - \bar{I} \langle \tau_{p+1} \rangle}{1 + (\omega \langle \tau_{p+1} \rangle)^2} \\ &\quad + 2 \frac{q_{p+1} - \bar{I} \langle \tau_{p+1} \rangle}{1 - i\omega \langle \tau_{p+1} \rangle} B_p, \end{aligned} \quad (\text{A12})$$

$$B_{p+1} = q_{p+1} - \frac{\bar{I} \langle \tau_{p+1} \rangle}{1 - i\omega \langle \tau_{p+1} \rangle} + B_p \frac{1}{1 - i\omega \langle \tau_{p+1} \rangle}. \quad (\text{A13})$$

(The initial conditions are still $A_0 = B_0 = 0$).

However, this improvement still does not solve the problem of relatively poor convergence of the algorithm, especially at low frequencies. The origin of the problem is hinted at by Eq. (A2). Since we eliminated the T -segmentation used in the standard method, and now T is much longer (the whole simulation period), we are calculating $S_I(\omega)$ with a much smaller degree of spectral smoothing. The price for a better spectral resolution $\Delta\omega$ is the longer simulation time for the same accuracy. Therefore, to improve convergence, we have to re-introduce some time constant T_0 that would define the spectral smoothing $\Delta\omega \sim 1/T_0$. In principle, there are many ways to do this. For example, we can periodically

(with period T_0) set to zero the value of B_p (in this case the algorithm becomes somewhat similar to the standard method). Alternatively, we can introduce a gradual cut-off of B_p , for example, multiplying the last term in Eq. (A13) by $\exp(-\langle\tau_{p+1}\rangle/T_0)$, and so on.

We have used the following way of introducing T_0 , which is the best among those we had tried. For simplicity, let us consider first the algorithm without subtraction of \bar{I} , and average Eq. (A6) over frequency (from $\omega = -\infty$ to $\omega = \infty$) with the Lorentzian weight factor $(T_0/\pi) / [1 + (\omega - \tilde{\omega})^2 T_0^2]$. The integral can be easily calculated using the residue theorem since all the poles of Eq. (A6) are in the lower half of the complex plane; therefore, closing the integration contour in the upper half-plane, we will have only one pole at $\omega = \tilde{\omega} + i/T_0$. As a result, the only change in Eq. (A6) after integration is that ω is replaced by $\omega + i/T_0$ (more correctly, by $\tilde{\omega} + i/T_0$, but for simplicity we change the notation from $\tilde{\omega}$ back to ω). Therefore, the Lorentzian averaging over frequency in our algorithm exactly corresponds to replacing ω with $\omega + i/T_0$ in the iteration equations (A9)–(A10).

For the algorithm with \bar{I} subtraction, the Lorentzian averaging is a little more difficult, because of the extra poles in the equation for $\langle s \rangle$ at $\omega = i/\langle\tau_k\rangle$ (upper half-plane) and at $\omega = 0$. However, as seen from Eqs. (A12)–(A13), the pole at $\omega = 0$ is eventually canceled, while the poles at $\omega = i/\langle\tau_k\rangle$ remain only in the simple additive term in Eq. (A12). Therefore, the recipe of replacing ω with $\omega + i/T_0$ still works for B_{p+1} , and the extra residue of the upper-half-plane pole should be simply added to A_{p+1} . As a result, Eqs. (A12)–(A13) are replaced with

$$A_{p+1} = A_p + q_{p+1}^2 + 2 \frac{q_{p+1} - \bar{I} \langle\tau_{p+1}\rangle}{1 - i(\omega + i/T_0) \langle\tau_{p+1}\rangle} B_p - \frac{2\bar{I} \langle\tau_{p+1}\rangle (q_{p+1} - \bar{I} \langle\tau_{p+1}\rangle) (1 + \langle\tau_{p+1}\rangle/T_0)}{1 + (\omega \langle\tau_{p+1}\rangle)^2 + 2\langle\tau_{p+1}\rangle/T_0 + (\langle\tau_{p+1}\rangle/T_0)^2}, \quad (\text{A14})$$

$$B_{p+1} = q_{p+1} - \frac{\bar{I} \langle\tau_{p+1}\rangle}{1 - i(\omega + i/T_0) \langle\tau_{p+1}\rangle} + B_p \frac{1}{1 - i(\omega + i/T_0) \langle\tau_{p+1}\rangle}, \quad (\text{A15})$$

while the rest of the algorithm does not change.

The introduction of Lorentzian smoothing greatly improves the convergence of the algorithm. However, it gives rise to another difficulty. The problem is that the averaging over frequency increases the δ -function contribution from $S_I(0)$ due to average current, and the trick of the standard method, discussed above, is impossible for Lorentzian averaging [in contrast to Eq. (A2), in which the convolution function contains zeros]. Formally, our algorithm subtracts \bar{I} beforehand; however, in a real simulation \bar{I} is not known exactly (note that the estimated value of \bar{I} can be improved during the course of simulation). It can be shown that the inaccuracy ΔI in the average current estimate used in Eqs. (A14)–(A15) brings to $S_I(\omega)$ the extra contribution

$$\Delta S_I(\omega) = 4T_0 (\Delta I)^2 / (1 + \omega^2 T_0^2). \quad (\text{A16})$$

This contribution can be subtracted from $S_I(\omega)$ at the end of the simulation run, when a better estimate of \bar{I} is known and the difference from the initially used estimate can be calculated. Actually, the value of \bar{I} used in Eqs. (A14)–(A15) can be periodically (sufficiently rare) updated during the simulation run; in this case $(\Delta I)^2$ in Eq. (A16) can naturally be replaced with the time-weighted value.

With these modifications, the advanced algorithm becomes significantly faster and more convenient than the standard algorithm. Accurate comparison of their efficiencies is not straightforward because both methods have adjustable parameters (T in the standard method and T_0 in the new method both affect the smoothing of the spectral density and the convergence speed; the choice of too short T could also lead to incorrect results). Crudely, the speed up factor (the ratio of CPU times for the same accuracy using the two methods) for our typical simulation runs is up to two or three orders of magnitude.

¹ N. F. Mott and J. H. Davies, *Electronic Properties of Non-Crystalline Materials*, 2nd Ed., (Oxford Univ. Press, Oxford, 1979); N. F. Mott, *Conduction in Non-Crystalline Materials*, 2nd Ed. (Clarendon Press, Oxford, 1993).
² B. I. Shklovskii and A. L. Efros, *Electronic Properties of Doped Semiconductors* (Springer, Berlin, 1984).
³ *Hopping Transport in Solids*, edited by A. L. Efros and M. Pollak (Elsevier, Amsterdam, 1991).
⁴ Ya. Blanter and M. Buttiker, Phys. Repts. **336**, 2 (2000).
⁵ K. A. Matsuoka and K. K. Likharev, Phys. Rev. B **57**, 15613 (1998).
⁶ A. N. Korotkov and K. K. Likharev, Phys. Rev. B **61**, 15975 (2000).

⁷ V. A. Sverdlov, A. N. Korotkov, and K. K. Likharev, Phys. Rev. B **63**, 081302(R) (2001).
⁸ Notice that in contrast with some prior works, we do not include the factor 2 in the exponent. This difference should be kept in mind at the level of result comparison.
⁹ N. S. Bakhvalov, G. S. Kazacha, K. K. Likharev, and S. I. Serdyukova, Sov. Phys. JETP **68**, 581 (1989).
¹⁰ C. Wasshuber, *Computational Single-Electronics* (Springer, Berlin, 2001), Ch. 3.
¹¹ W. Brenig, G. H. Döhler, and H. Heyszenau, Phil. Mag. **27**, 1093 (1973).
¹² D. N. Tsigankov and A. L. Efros, Phys. Rev. Lett. **88**, 176602 (2002).

- ¹³ For a discussion of this issue, see Sec. 4.2 of Ref. 2.
- ¹⁴ S. Marianer and B. I. Shklovskii, Phys. Rev. B **46**, 13100 (1992).
- ¹⁵ B. I. Shklovskii, Fiz. Tekh. Poluprovodn. **6**, 2335 (1972) [Sov. Phys. Semicond. **6**, 1964 (1973)].
- ¹⁶ This result emphasizes again that the validity of the master equation approach is very limited, and for most transport characteristics this equation fails to give quantitatively correct results for any region in the $[E, T]$ space.
- ¹⁷ M. Amman, K. Mullen, and E. Ben-Jacob, J. Appl. Phys. **65**, 339 (1989).
- ¹⁸ A. N. Korotkov, D. V. Averin, K. K. Likharev, and S. A. Vasenko, in *Single-Electron Tunneling and Mesoscopic Devices*, edited by H. Koch and H. Luebbig (Springer, Berlin, 1992), p. 45.
- ¹⁹ A. N. Korotkov, Phys. Rev. B **49**, 10381 (1994).
- ²⁰ B. I. Shklovskii, Solid State Commun. **33**, 273 (1980); Sh. M. Kogan and B. I. Shklovskii, Sov. Phys. Semicond. **15**, 605 (1981).
- ²¹ B. I. Shklovskii, Phys. Rev. B **67**, 045201 (2003).
- ²² D. Stauffer and A. Aharony, *Introduction to Percolation Theory*, Rev. 2nd Ed., (Taylor and Francis Inc, Philadelphia, 1994).
- ²³ S. P. Obukhov, Physica A **101**, 145 (1980).
- ²⁴ J. W. Essam, K. De'Bell, J. Adler, and F. M. Bhatti. Phys. Rev. B **33**, 1982 (1986).
- ²⁵ V. V. Kuznetsov, E. E. Mendez, X. Zuo, G. Snider, and E. Croke, Phys. Rev. Lett. **85**, 397 (2000).
- ²⁶ S. H. Roshko, S. S. Safonov, A. K. Savchenko, W. R. Tribe, and E. H. Linfield, Physica E **12**, 861 (2002).
- ²⁷ B. Derrida, Phys. Reports **301**, 65 (1998).
- ²⁸ K. Likharev, Proc. IEEE **87**, 606 (1999).
- ²⁹ V. A. Sverdlov, D. M. Kaplan, A. N. Korotkov, and K. K. Likharev, Phys. Rev. B **64**, 041302(R) (2001).
- ³⁰ D. V. Averin and K. K. Likharev, in *Mesoscopic Phenomena in Solids*, edited by B. L. Altshuler, P. A. Lee, and R. A. Webb (Elsevier, Amsterdam, 1991), p. 173.
- ³¹ MOSES - Monte-Carlo Single-Electron Simulator, versions 1.11 (for DOS and UNIX) and 1.2 (for UNIX only) are available at <http://hana.physics.sunysb.edu/set/software/index.html>.